Spatially-resolved mapping of history-dependent coupled electrochemical and electronical behaviors of electroresistive NiO

Issei Sugiyama[1], Yunseok Kim[2], Stephen Jesse[3], Evgheni Strelcov[3], Amit Kumar[4], Alexander Tselev[3], Ehasan Kabiri Rahani[5], Vivek B. Shenoy[5], Takahisa Yamamoto[1,6,7], Naoya Shibata*[1,8], Yuichi Ikuhara[1,7,9], Sergei V. Kalinin*[3,10]

[1]Institute of Engineering Innovation, The University of Tokyo, Yayoi 2-11-16, Bunkyo-ku, Tokyo, Japan, 113-8656

[2]School of Advanced Materials Science and Engineering, Sungkyunkwan University, Cheoncheon-dong 300, Jangan-gu, Suwon, Gyeonggi-do 440-746, Republic of Korea

[3]The Center for Nanophase Materials Sciences, Oak Ridge National Laboratory, Oak Ridge, Tennessee 37831-6496, United States

[4]School of Mathematics and Physics, Queen's University Belfast, University Road Belfast, Northern Ireland, BT7 1NN, United Kingdom

[5]Department of Materials Science and Engineering, University of Pennsylvania, Philadelphia PA, 19104-6272.

[6]Department of Quantum Engineering, Nagoya University, Furo-cho, Chiho-ku, Nagoya-shi, Aichi, Japan, 464-8603

[7]Nanostructures Research Laboratory, Japan Fine Ceramics Center, Rokuno 2-4-1, Atsuta-ku, Nagoya-shi, Aichi, Japan, 456-8587

[8]PRESTO Japan Science and Technology Agency, 4-1-8 Honcho Kawaguchi, Saitama 332-0012, Japan.

[9]WPI Advanced Institute for Materials Research, Tohoku University, Katahira 2-1-1, Aoba-ku, Sendai-shi, Miyagi, Japan, 980-8577

[10]Institute for Functional Imaging of Materials, Oak Ridge National Laboratory, Oak Ridge, Tennessee 37831-6496, United States

* shibata@sigma.t.u-tokyo.ac.jp and sergei2@ornl.gov

S.1 The structure of Pt pyramid

The pyramidal structure of Pt in NiO thin film can be confirmed by the following plan-view TEM observations. Fig. S1a shows magnified TEM bright field image of Pt pyramid seen from NiO (001). Moiré pattern is observed at the edge of Pt square pyramid. The periodicity of moiré pattern is about 8 nm. This is consistent with the lattice mismatch between NiO and Pt, so the NiO/Pt interface is observed at the area of moiré pattern. The thin foil for TEM observations is prepared by back thinning and subsequent gentle milling from both side as a finishing process. Hence the Pt pyramid in the thin foil for TEM observations is polished from both side as shown schematically in Fig. S1b. The area of moiré pattern observed in Fig. S1a is consistent with the NiO/Pt interfaces included in the thin foil for TEM observations expected from the sample morphology. From these discussions, the square Pt observed in NiO thin film is confirmed to be the pyramidal structure.

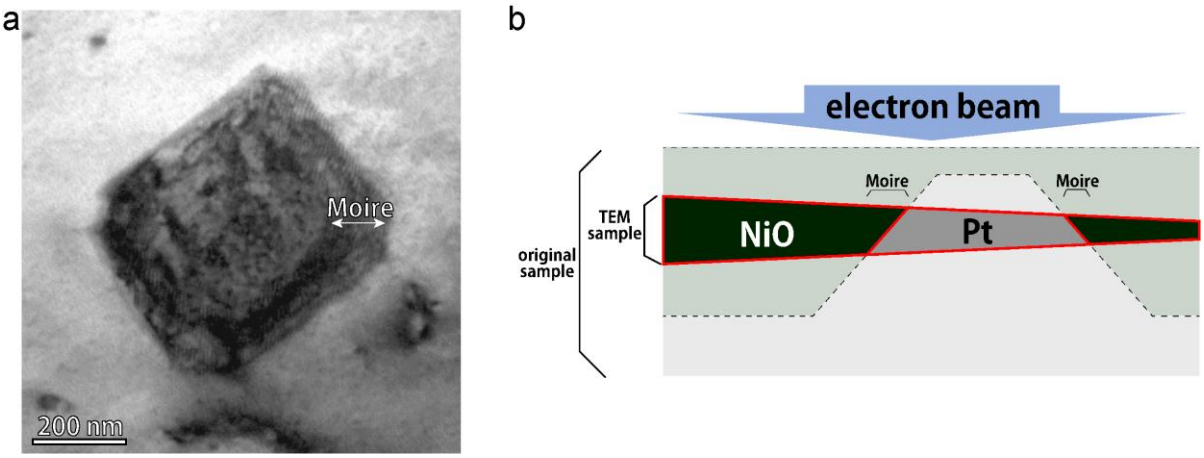

Fig. S1 | a TEM bright field image of Pt pyramid. **b** A schematic of the thin foil for TEM observations. Red lines represent for the TEM samples and dotted lines are original sample before thinning.

S.2 Crystallinity of the NiO film

Fig. S2 show out-of-plane XRD profile of the NiO film on Pt single crystalline substrate. Only the peaks of single crystalline NiO (001) and Pt (001) are observed. So this profile is clearly showing that the NiO film consist of single crystal, or at least, the film is highly oriented. The in-plane crystallinity can be checked by the TEM image and selected area diffraction pattern shown in Fig. S3. The image and pattern show the NiO film is consist of single crystal. From these XRD profile and TEM observations, the NiO film on the Pt single crystalline substrate are confirmed to be single crystal and the NiO (001) is parallel to Pt (001).

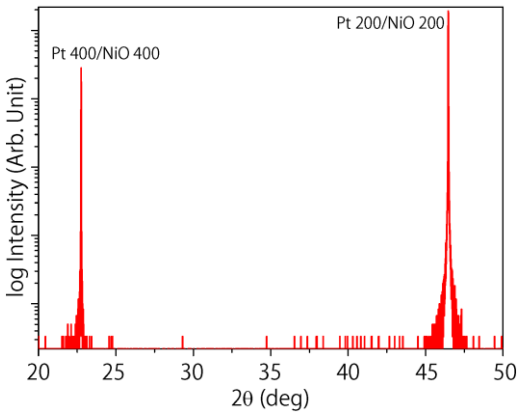

Figure S2 | XRD out-of-plane profile of NiO/Pt. Only the peak of Pt and NiO single crystal is detected.

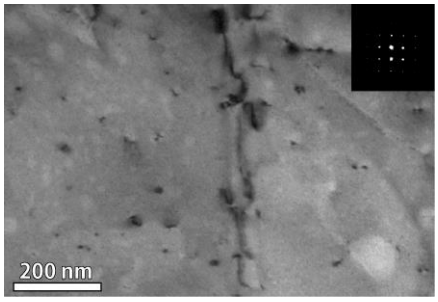

Figure S3 | TEM bright field image of NiO film observed from plan-view NiO (001) direction. The inlet show selected area diffraction pattern at the area of the image.

S.3 Dominant defects in conductive path formation

Although both nickel vacancies and oxygen vacancies can be formed in NiO, many studies report that the eledctroresistive phenomena is according to the oxygen vacancies [1-3]. The oxygen vacancies can be formed in the following equation [4]:

$$O_O + Ni_{Ni} \rightleftarrows V_O^{\cdot\cdot} + Ni_{Ni}'' + {}^1/_2\, O_2 \qquad \text{(Eq. S1)}$$

where $V_O^{\cdot\cdot}$ are oxygen vacancies and Ni_{Ni}'' is the Ni^{2+} site with two extra electrons (i.e. a neutral Ni atom).

In ESM hysteresis as in Fig. 3d, the dominant defects can be confirmed by the form of hysteresis loop. The charge of oxygen vacancies are opposite to that of nickel vacancies, so the behavior of oxygen vacancies must be opposite to that of nickel vacancies. This fact means that the hysteresis loops formed by the oxygen vacancies dominating phenomena and the loops formed by the nickel vacancies dominating phenomena are in relationship of upside-down. In the case of NiO, the hysteresis loop in Fig. 3d is known to be according to the oxygen vacancies [5]. So the discussions in the manuscript are assuming oxygen removal in the (Eq. S1) following Ref. [4].

Although the dominant defects are concluded to be the oxygen vacancies from the experimental results, the story is not affected if the dominant defects were nickel vacancies. Assuming the nickel vacancies are formed in the following equation [6,7]:

$$2Ni_{Ni} + {}^1/_2\, O_2 \rightleftarrows 2Ni_{Ni}^{\cdot} + V_{Ni}'' + O_O \qquad \text{(Eq. S2)}$$

Here, the difference of dominant defects only affect the constant in the Eq. (1) in the main part of the manuscript. The spatial point dependent variable is only related to the strain. So the relative value of color map in Fig. 8(b) must be the same whether the dominant defects are oxygen vacancies or nickel vacancies, although the absolute value

can be varied. The discussions in this study is based only on the relative value in Fig. 8(b). Hence the discussions in this study is not affected by the vacancy species.

References

[1] Lee, M.H., *et al.* Scanning probe based observation of bipolar resistive switching NiO films. *Appl. Phys. Lett.* **97**, 062909 (2010).

[2] Yoshida, C., Kinoshita, K., Yamasaki, T. & Sugiyama, Y. Direct observation of oxygen movement during resistance switching in NiO/Pt film. *Appl. Phys. Lett.* **93**, 042106 (2008).

[3] Lee, S.R., *et al.* Role of oxygen vacancies formed between top electrodes and epitaxial NiO films in bipolar resistance switching. *Curr. Appl. Phys.* **12**, 369-372. (2012).

[4] Kim, Y., *et al.* Mechanical Control of Electroresistive Switching. *Nano Lett.* **13**, 4068-4074. (2013).

[5] Kim Y., *et al.* Correlative Multimodal Probing of Ionically-Mediated Electromechanical Phenomena in Simple Oxides. *Sci. Rep*. **3**, 2924 (2013).

[6] Koel, G.J., & Gellings, P.J. The Contribution of Different Types of Point Defects to Diffusion in CoO and NiO During Oxidation of the Metals. *Oxidation Metal.* **5**, 185-203 (1972).

[7] Christian, J.D., Gillbreath, W.P. Defect Structure of NiO and Rates and Mechanisms of Formation from Atomic Oxygen and Nickel. *Oxidation Metal.* **9**, 1-25. (1975).

S.4 Finite element calculations details

A finite element analysis has been carried out to reveal the stress distributions and oxygen vacancies and extra electron distributions. A schematic of the calculated model is shown in Fig. S4. The stress according to the lattice mismatch is modelled virtually by the difference of thermal expansion coefficient between NiO and Pt. The sample is virtually heated up to 1200 K so that the stress correspond to that introduced by lattice mismatch will be introduced. The stress analysis equilibrium equation coupled with the defects induced strains due to volume change and thermal strain are as follows:

$$\nabla \cdot \sigma = 0 \qquad \text{(Eq. S3)}$$

$$\begin{gathered} \sigma = \mathrm{C} : \left(\varepsilon - \epsilon_{defect} - \varepsilon_{thermal}\right) \\ \varepsilon = \frac{1}{2}\left[(\nabla u)^T - \nabla u\right] \\ \varepsilon_{defect} = \frac{1}{3V_m}\{\bar{V}_v[c_v(x,y,z) - c_v^{\infty}] + \bar{V}_e[c_e(x,y,z) - c_e^{\infty}]\} \\ \varepsilon_{thermal} = \alpha_T\left(T - T_{ref}\right) \end{gathered} \qquad \text{(Eq. S4)}$$

where $c_e^{\infty} = c_v^{\infty}$ are oxygen vacancy and extra electron concentrations in bulk.

c_v and c_e are defined as [1]:

$$\begin{aligned} \mathrm{c}_v(x,y,z) = c_v^{\infty}\exp\left\{\frac{\bar{V}_v}{3RT}\left[\sigma_x(x,y,z) + \sigma_y(x,y,z)\right.\right. \\ \left.\left. + \sigma_z(x,y,z)\right]\right\}\exp\left\{\frac{-2F}{RT}\Delta\phi(x,y,z)\right\} \\ \mathrm{c}_e(x,y,z) = c_e^{\infty}\exp\left\{\frac{\bar{V}_e}{3RT}\left[\sigma_r(x,y,z) + \sigma_\theta(x,y,z)\right.\right. \\ \left.\left. + \sigma_z(x,y,z)\right]\right\}\exp\left\{\frac{+2F}{RT}\Delta\phi(x,y,z)\right\} \end{aligned} \qquad \text{(Eq. S5)}$$

where $\Delta\phi(x,y,z) = \phi(x,y,z) - \phi^{\infty}$, $\Delta\phi(x,y,0) = \Delta\phi_0$. The details of parameters are summarized in Table S1.

As shown in Fig.8a, the maximum average stress $\sigma_x + \sigma_y$ occurs around the pyramid tip and it is expected to be enhanced above four tip corners. We see from Eq.S3 that c_e depends exponentially on the average stress : ce~exp $\left(\frac{\bar{V}_e}{3RT}[\sigma_x + \sigma_y]\right)$. Thus ce is significantly enhanced on the surface plane above the pyramid tip where lobes are formed at the four corners similar to what is observed experimentally.

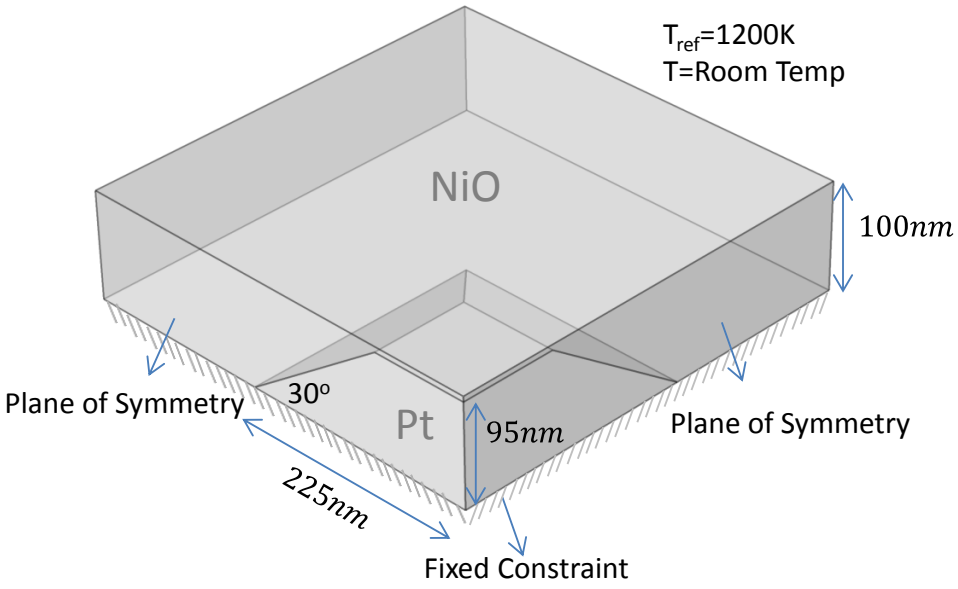

Figure S4 | A 3D schematic of model for finite element calculations.

Table S1 | List of parameters used for finite element modeling.

Parameter	Definition	Value	Comments
E_m	Young's modulus of NiO	169 GPa	Refs. [2, 3]
ν_m	NiO Poisson's ratio	0.3	Refs. [2, 3]
c_e^{∞}	Bulk Oxygen vacancy concentration	0.01	Assumed
$\bar{V}_e$	partial molar volumes for extra	8.19 cm^3/mol	Assumed

	electron		
V_m	molar volume of stoichiometric NiO	11.198 cm^3/mol	Calculated
ϵ_r	The relative dielectric permittivity of NiO	11.75	Ref. [4]
T	Temperature	293 K	From literature
T_{ref}	Reference Temperature	1200 K	From Experiment
β	See Eq.7	2.7	Assumed
$\Delta\phi_0$	fixed surface potential	0.0 V	Assumed
α_{T,N_iO}	Thermal expansion coefficient for NiO	1.2351E-5 (1/K)	Refs. [2, 3]
α_{T,P_t}	Thermal expansion coefficient for Pt	8.80E-6 (1/K)	Refs. [2, 3]

References

[1] Sheldon, B. W. and Shenoy, V. B. Space Charge Induced Surface Stresses: Implications in Ceria and Other Ionic Solids. *Phys. Rev. Lett.* **106**, 216104 (2011).

[2] Every, A. G. McCurdy, A. K. Elastic in *1.2.1 constants s, c*, edited by D. F. Nelson, Vol. 29a.

[3] Plessis, P. D. V. D.. Tonder, S. F. V. and Alberts, L. Elastic constants of a NiO single crystal: I. *J. Phys. C: Solid St. Phys.* **4**, 1983-1987 (1971).

[4] Gielisse, P. J., *et al.* Infrared Properties of NiO and CoO and Their Mixed Crystals. *J. Appl. Phys.* **36**, 2446-2450 (1965).